

Down-Hole Electromagnetic Heating of Deep Aquifers for Renewable Energy Storage

Oliveira de Almeida, Samuel; Chapiro, Grigori; Zitha, Pacelli L.J.

DOI

[10.3390/en15113982](https://doi.org/10.3390/en15113982)

Publication date

2022

Document Version

Final published version

Published in

Energies

Citation (APA)

Oliveira de Almeida, S., Chapiro, G., & Zitha, P. L. J. (2022). Down-Hole Electromagnetic Heating of Deep Aquifers for Renewable Energy Storage. *Energies*, 15(11), Article 3982. <https://doi.org/10.3390/en15113982>

Important note

To cite this publication, please use the final published version (if applicable). Please check the document version above.

Copyright

Other than for strictly personal use, it is not permitted to download, forward or distribute the text or part of it, without the consent of the author(s) and/or copyright holder(s), unless the work is under an open content license such as Creative Commons.

Takedown policy

Please contact us and provide details if you believe this document breaches copyrights. We will remove access to the work immediately and investigate your claim.

Article

Down-Hole Electromagnetic Heating of Deep Aquifers for Renewable Energy Storage

Samuel O. de Almeida ^{1,*} , Grigori Chapiro ^{2,*}  and Pacelli L. J. Zitha ^{3,*} ¹ Federal Institute of the Southeast of Minas Gerais, Santos Dumont 36240-000, Brazil² Department of Mathematics, Federal University of Juiz de Fora, Juiz de Fora 36036-900, Brazil³ Civil Engineering and Geosciences, Delft University of Technology, 2628 CD Delft, The Netherlands

* Correspondence: samuel.oliveira@ifsudestemg.edu.br (S.O.d.A); grigori@ice.ujf.br (G.C.);

p.l.j.zitha@tudelft.nl (P.L.J.Z.)

Abstract: Electromagnetic (EM) heating is an emerging method for storing renewable energy, such as photovoltaic solar and wind electric power, into aquifers. We investigate how the captured energy increases the temperature of a prototypical deep aquifer for a six-month period and then to which extent the stored energy can be recovered during the consecutive six months. Water injected at a constant flow rate is simultaneously heated using a high-frequency electromagnetic microwave emitter operating at the water natural resonance frequency of 2.45 GHz. The coupled reservoir flow and EM heating are described using Darcy's and the energy balance equations. The latter includes a source term accounting for the EM wave propagation and absorption, modeled separately using Maxwell's equations. The equations are solved numerically by the Galerkin least-squares finite element method. The approach was validated using EM-heating input data obtained from controlled laboratory experiments and then was applied to the aquifer. We found that after six years of alternate storage and recovery, up to 77% of the injected energy is recovered when considering realistic heat losses estimated from field data. Even when heat losses are increased by a factor of two, up to 69% of the injected energy is recovered in this case. This shows that down-hole EM heating is a highly effective method for storing renewable energies, capable of helping to solve their inherent intermittency.

Keywords: low-enthalpy geothermal sources; electromagnetic heating; flows in porous media; partial differential equations



Citation: Almeida, S.O.d.; Chapiro, G.; Zitha, P.L.J. Down-Hole Electromagnetic Heating of Deep Aquifers for Renewable Energy Storage. *Energies* **2022**, *15*, 3982. <https://doi.org/10.3390/en15113982>

Academic Editor: Anna Sowizdzal

Received: 30 March 2022

Accepted: 30 April 2022

Published: 28 May 2022

Publisher's Note: MDPI stays neutral with regard to jurisdictional claims in published maps and institutional affiliations.



Copyright: © 2022 by the authors. Licensee MDPI, Basel, Switzerland. This article is an open access article distributed under the terms and conditions of the Creative Commons Attribution (CC BY) license (<https://creativecommons.org/licenses/by/4.0/>).

1. Introduction

In the last decade, the significance of solar and wind energy sources has grown considerably under the societal pressure to curb CO₂ emissions imputable to the use of natural hydrocarbons. Solar power plants generate substantial amounts of energy, but mostly during daytime and in summer, and wind-turbine energy output depends on weather conditions. This is in stark contrast with the energy consumption profile in the built environment, which is higher at later parts of the day and in the colder seasons [1]. Resolving this intermittency conundrum of solar and wind energies is essential for a wider acceptance and usage of these renewable energy sources.

Aquifer thermal energy storage (ATES) seeks to increase the efficiency of the terrestrial energy system by storing heated water in the subsurface; see [2]. One of the simplest forms of the ATES system consists of two underground wells that operate cyclically between summer and winter [3]. In summer, cold water is extracted from the aquifer and is generally used for cooling buildings and industrial processes, and then is reinjected into the aquifer through the storage well. In winter, the reverted water flows in any direction possible in the heating buildings and industries. ATES techniques are based on heated water injection; the majority in shallow reservoirs, and a few others in medium/deep aquifers [3–5]. Notice that the latter type is more affected by heat losses.

Hybrid energy systems combining low-enthalpy (low-H) geothermal sources, i.e., aquifers with temperatures below 90 °C, with wind or solar energy, were studied by [6–9]. The geothermal sources can potentially provide an enormous energy storage capacity [10] while enhancing the overall efficiency of the energy supply [11,12]. Nevertheless, there is still a lack of data and models concerning this process for high depths. The present paper follows a similar idea by considering energy storage at deep reservoirs, where thermal losses can play a significant role. Including these types of aquifers increases renewable energy usage.

Subsurface EM heating is not completely new [13–15]. It has been a subject of several studies mainly in the context of clean-up of polluted soils [16], and enhanced oil recovery (EOR) [17–20]. However, it is far from being completely understood, especially in the context of geothermal energy sources. For instance, the impact of EM propagation on the efficiency of energy storage and the role of the various energy losses have not been discussed in detail. Electromagnetic heating is hardly affected by the heterogeneity of the reservoir and allows uniform heat distribution in the medium [21]. In addition, compact and high-efficiency EM heating equipment allows a more straightforward setup inside the well. The experiments reported in [22] showed that heat could be induced from the inside out, while [23] demonstrated that it is possible to obtain heating faster when compared to traditional thermal techniques, resulting in less heat loss due to the greater penetration in the medium. Authors report similar results in [24], stating that the EM heating is advantageous in avoiding thermal losses when compared to traditional thermal methods such as hot water (or steam) injection. Numerical and analytical study [25], considering thermal losses proposed in [26], was performed calculating the heat loss for adjacent extracts considering heat conduction. Similarly, vertical heat losses for over- and underburden formations were modeled through the heat diffusion equation [27].

After the model validation on the data obtained from the laboratory-controlled experiments, we conducted a numerical analysis of the energy storage and recovery from an aquifer based on a coupled EM heating and reservoir flow mathematical model. As illustrated in Figure 1, we apply the model to assess the efficiency in six-month cycle production and storage for a total duration of six years. The paper proceeds with the physical model, numerical details, and results and discussion, followed by conclusions. For completeness, we present the approach validation in the Appendix, although it can also be found in [28].

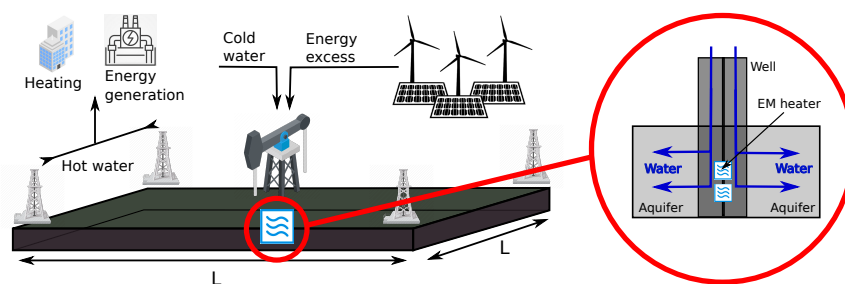


Figure 1. Schematic representation of the proposed scheme.

2. Physical Model

Consider a solar and wind power electrical power source and a well drilled into an aquifer, as depicted in Figure 1. A source of EM waves operating in the microwave at wavelengths is placed at the bottom of the well to enable energy to be injected directly into the reservoir [29]. This configuration clearly minimizes the heat losses due to energy transfer along the walls of the injection well and maximizes the total amount of energy reaching the reservoir. Our discussion will be confined to the less-evident EM propagation in the reservoir.

To fix ideas, we assume the reservoir to be a homogeneous and isotropic reservoir with porosity ϕ and permeability k and dimensions $L \times L \times h$. In addition to the injection well already mentioned, four wells are drilled at the edges of the reservoir so that altogether

they form a five-spot configuration (see Figure 1). The well diameter is considered equal to 27.3 cm (or 10 3/4 in), one of the standard casing diameters. Water at temperature θ_0 is injected into the aquifer at a flow rate Q_w and a constant pressure gradient, while the microwave emitter irradiates energy with nominal power W . From the physical point of view, we need to solve the problem of the flow of water into the reservoir coupled with the heat transfer with an EM source.

This work's premise is that the energy stored in the aquifer can be recovered through the four production wells. Since flow and temperature profiles are symmetrical with respect to the central well's axis, we present only the first quadrant of the simulation.

Note that heating of shallow aquifers should not exceed 30 °C (LT-ATES) due to environmental, economic, and social risks; see [5] for details. We consider deep aquifers with high temperature and pressure, although we limit this study to reservoir temperature below 365.7 °C and pressures over 20 MPa to avoid the possibility of steam formation. When working with deep aquifers, the risks of harm to the environment are lower. Another factor is the presence of multiple rock layers overlying the aquifer, which will limit the vertical heat flow and chemical transport to the surface. In fact, high temperatures occur naturally at these depths in various parts of the world due to relative proximity to the Earth's core.

2.1. Governing Equations

Fluid flow in the aquifer is governed by mass, momentum, and energy conservation. For porous media flow, the momentum equation reduces to Darcy's law; see [30,31]. As we deal with a reservoir-scale phenomenon with a significant timescale (months), we assume that flow is incompressible and in the steady state. The mass conservation equations and Darcy's law can be combined into the following pressure equation:

$$\nabla \cdot \left(\frac{k}{\nu} \nabla p \right) = 0, \quad \text{where} \quad \log \nu = a_1 + \frac{a_2}{(a_3 - \theta)}, \quad (1)$$

where k is the permeability of the porous medium, ν is the viscosity of water depending on temperature θ [32], and p is the local pressure in the reservoir.

The energy balance is expressed by the following heat convection–diffusion equation [20,33,34]:

$$C_t \frac{\partial \theta}{\partial t} + C_w \nabla \cdot (V\theta) = K_t \Delta \theta - C_l (\theta - \theta_0) + W, \quad (2)$$

where velocity V is obtained from Darcy's equation using pressure field from Equation (1), C_t is the system's specific heat, C_w is the total fluid specific heat, K_t is the total system thermal conductivity, C_l is the thermal losses coefficient, and W is the total electromagnetic energy source. Note that, for simplicity, the thermal expansion of the rock and the fluids are assumed to be negligible, which is an acceptable approximation for the range of temperature variations considered in this study. The temperature in the reservoir rises due to heat conduction, convection, and radiation. Using the relationships between volume fraction, saturation, total Darcy velocity, and flow function, we can write the coefficients as

$$C_t = \phi \rho_w c_w + (1 - \phi) \rho_s c_s, \quad (3)$$

$$C_w = \rho_w c_w + \rho_s c_s, \quad (4)$$

$$K_t = \phi k_w + k_s (1 - \phi). \quad (5)$$

Note that, consistently with Equation (2), the amount of heat transferred by conduction q (W) in the unit of time inside the material in the vertical direction is given by Fourier thermal conduction law:

$$q = K_t A d_z \theta, \quad (6)$$

where K_t is the thermal conductivity ($W/(m \text{ K})$), and A (m^2) is the area of the section perpendicular to the flow's direction. Equating the total energy loss, calculated by using

(6), for $L \times L \times h$ reservoir's size (length, width, and height), with the same using the linear thermal loss coefficient C_l , we arrive at $C_l = K_t/h^2$.

2.2. EM Heating

The detailed derivation of the total electromagnetic energy source W of electromagnetic heating from the Maxwell equations can be found in [28]. Here, we recall the main result, which can be expressed as

$$W(r) = \frac{P_0}{2\pi h} \left[2\alpha \frac{e^{-2\alpha(r-r_w)}}{r} + \frac{e^{-2\alpha(r-r_w)}}{r^2} \right], \quad (7)$$

where P_0 is the incidence power, h is the reservoir height, r is the radius, and r_w is the wellbore radius. The attenuation factor is given by

$$\alpha = \omega \sqrt{\frac{\mu_0 \mu_r \varepsilon_0 \varepsilon_r}{2} \left(\sqrt{1 + \left(\frac{\sigma}{\mu \varepsilon_0 \varepsilon_r} \right)^2} - 1 \right)}, \quad (8)$$

where ω is the angular frequency, μ_0 and μ_r are vacuum and relative magnetic permeabilities, ε_0 and ε_r are vacuum and relative electric permittivities, and σ is the medium conductivity.

3. Numerical Methods

We solve the system of Equations (1) and (2) to simulate the heating of a $100 \text{ m} \times 100 \text{ m}$ aquifer with five wells in a five-spot configuration.

The two cases having practical significance considered are (a) continuous water injection and EM heating, where EM heater is placed inside the vertical injection well located in the center of the aquifer, and (b) alternated water injection and EM heating; in this case, the wells are alternatively switched from injectors to producers and vice versa (see Figure 2). Both configurations were simulated using parameters described in Table 1, which were obtained from the literature [20,32,35,36].

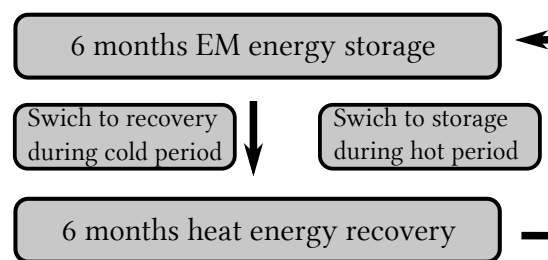


Figure 2. Schematic representation of the proposed energy storage through EM heating.

We use an efficient numerical scheme based on the Galerkin least-squares finite element method (GLS) to solve Equations (1) and (2) [37]. GLS possesses the accuracy of the standard Galerkin method and the stability of the least-squares method. It consists of determining the equations' variational formulation, approximating the solution by a different family of polynomial base functions when high convection occurs alongside low diffusion.

A staggered algorithm is employed to solve the system of partial differential equations by decoupling it into subsystems solved sequentially. This scheme is commonly used when equations express different physics; see [38].

Table 1. Physical parameters used in calculations.

Symbol	Physical Quantity	Value	Unit (SI)
ϕ	porosity	0.220	[-]
s_w	water saturation	1	[-]
ν_w	water viscosity	1.002×10^{-3}	[Pa·s]
ρ_s	porous media density	2.650×10^3	[Kg/m ³]
ρ_w	water density	0.997×10^3	[Kg/m ³]
c_s	PM specific heat capacity	0.920×10^3	[J/Kg·K]
c_w	water specific heat capacity	4.2×10^3	[J/Kg·K]
k_s	PM thermal conductivity	2.30	[W/m·K]
k_w	water thermal conductivity	0.58	[W/m·K]
L	reservoir length and width	100	[m]
Q_w	flux rate	4×10^{-5}	[m/s]
A	cross section	1.7	[m ²]
h	reservoir height	5	[m]
P	power of the EM emitter	18.5	[kW]
θ_0	initial temperature	308.15	[K]
k	permeability	700	[mD]
a_1	constant Equation (1)	-4.53	[-]
a_2	constant Equation (1)	-220.53	[-]
a_3	constant Equation (1)	149.39	[-]
ϵ_0	vacuum electric permittivity	8.854×10^{-12}	[F/m]
ϵ_r	relative electric permittivity	81	[F/m]
μ_0	vacuum magnetic permeability	$4\pi \times 10^{-7}$	[H/m]
μ_r	relative magnetic permeability	1	[H/m]
σ	medium conductivity	0.02	[S/m]
ω	angular frequency	$2\pi f$	[rad/s]
α	water EM energy absorption	4.185×10^{-1}	[1/m]
C_t	system specific heat	2.822	[MJ/m ³ ·K]
C_w	total fluid specific heat	6.625	[MJ/m ³ ·K]
K_t	tot. system thermal conductivity	1.9216	[W/m·K]
C_l	thermal losses	0.02	[W/m ³ ·K]

Following this technique, we solve Equation (1) considering the injection well located at coordinate (0, 0) and the production well, located at coordinate (50, 50), at the opposite end following the aquifers' diagonal. Both wells are maintained at a constant flux Q_w , implemented as a constant flux Neumann boundary condition at injection/recovery wells and null flux Neumann at the rest of the boundary. As a result, we obtain the velocity field V . In the next step, we use V to solve Equation (2), considering the initial condition given by θ_0 with Dirichlet boundary condition equal to θ_0 in the injection well and null flux Neumann condition for the rest of the boundary. Here, we use the coefficients C_w , C_t , and K_t given by Equations (3)–(5), and the volumetric heat dissipation W given by Equations (7)–(8). As a result, we obtain a temperature profile θ . The procedure restarts by using θ to solve Equation (1), at the next time step, through implicit Euler's method.

The maximum relative error for the numerical method was obtained by comparing the energy balance between the power P of the EM emitter with the energy stored, recovered, and lost in the reservoir, obtained by the space–time integral of the first four terms of Equation (2). For a six-year time, the relative error of numerical simulations was estimated to be 1.2%.

4. Results and Discussion

Here, we present the results obtained in the two cases considered in Section 3. Our discussion will focus on the amount of energy stored in the aquifer and, especially for the second case, on the energy that can be recovered upon switching to the stored energy production. All simulations use parameter values described in Table 1.

4.1. Continuous Water Injection under EM Heating

Water at constant temperature of 35 °C is injected with constant Darcy’s velocity of 4×10^{-5} (m/s), which corresponds to the pressure gradient of approximately 0.07 MPa. Since the flow and temperature are symmetrical with respect to the central aquifer well, we present the reservoir temperature distribution only for the first quadrant in Figure 3. Figure 3a shows the 3D map of the obtained temperature distribution after 6 months’ continuous injection.

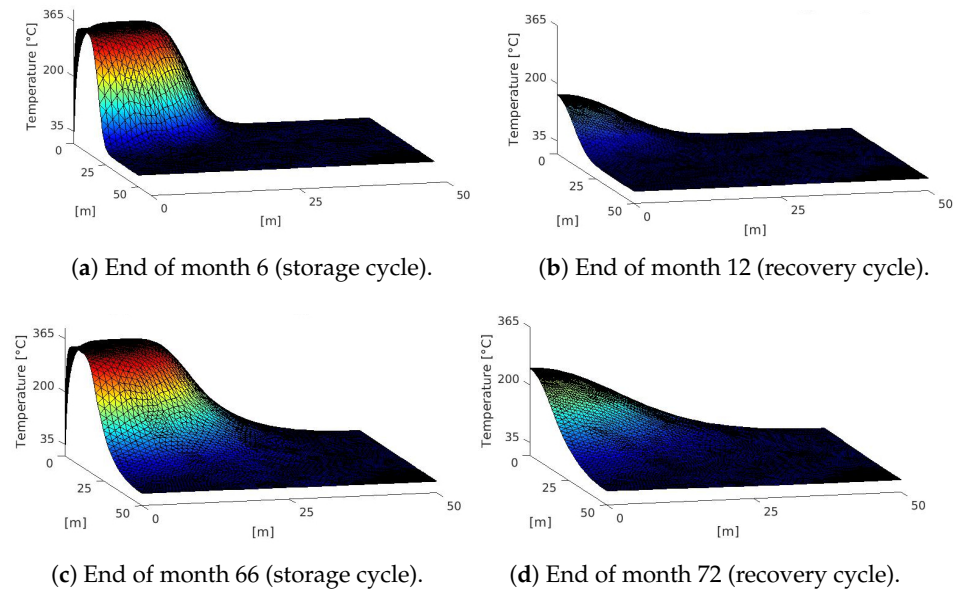


Figure 3. The temperature distribution inside the aquifer at different times: (a,b) correspond to the storage cycles; (c,d) correspond to the recovery cycles.

The temperature profiles in Figure 4a correspond to the diagonal section in Figure 3 for different times. Solid lines were obtained without thermal losses, while dashed lines were obtained with $C_l = 0.02$. As expected, after the heat wave moves towards the injection well, we notice a stabilization in the reservoir temperature over time. Considering small heat losses, the temperature profile shows deviation from the original one after three months, as can be observed in Figure 3a. The change in the temperature of the reservoir is stable during the energy storage cycle. As can be observed in Figure 3a, the traveling heat profile remains uniform over time with decreasing velocity. When thermal losses are considered, a small flattening of the heat front is observed. This temperature stability around the well allows a controlled and effective recovery in the subsequent cycle.

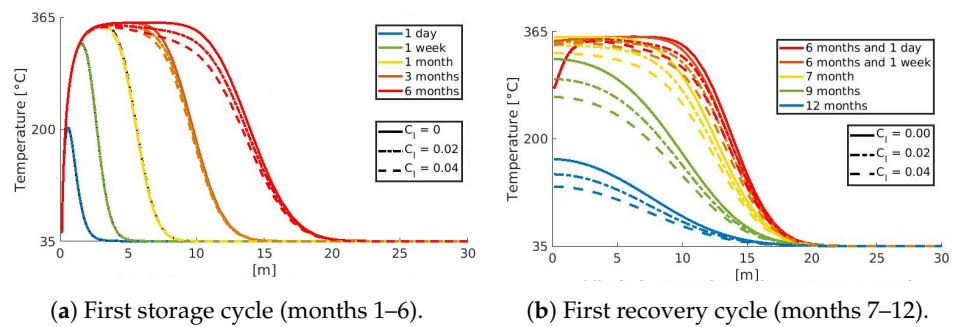


Figure 4. Cont.

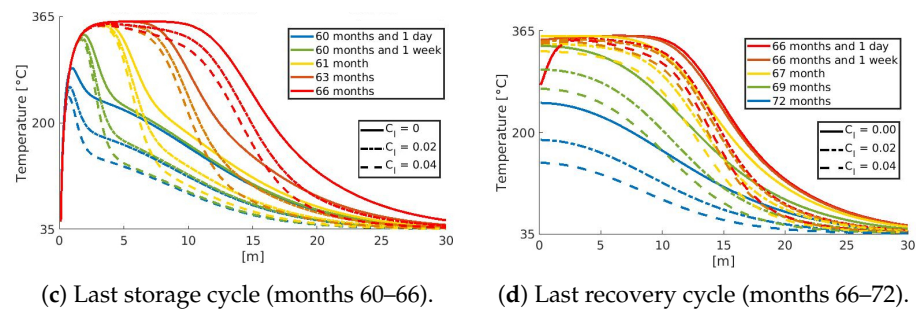


Figure 4. The temperature distribution along the diagonal section of the aquifer for different times. Storage cycles: (a,c). Recovery cycles: (b,d).

Temperature control is essential to avoid the formation of water vapor near the EM emitter as it has a lower thermal capacity and can cause overheating. The simulations show that the temperature rises considerably with decreasing the wellbore radius, and it decreases with the increase in water injection speed. Thus, controlling the emitter power and the injection flow rate is essential to maintain the temperature below 365.7 °C.

4.2. Energy Recovery

Following the case (b) from Section 3, we simulate the alternated water injection and EM heating in six-month cycles. The wells are alternatively switched from injectors to producers and vice versa. Figure 3b,d show the 3D temperature distribution inside the reservoir after 12 months (end of the first recovery cycle) and 72 months (end of the last recovery cycle). Figure 3c shows the 3D map of the obtained temperature distribution after 66 months at the end of the last storage cycle. The temperature profiles in Figure 4b,d correspond to the diagonal section of the reservoir part plotted in Figure 3b,d, respectively. The temperature profiles in Figure 4c correspond to the diagonal section in Figure 3c for different times during the last storage cycle. As before, these profiles were plotted neglecting thermal losses ($C_l = 0$), using thermal losses estimated for this reservoir in Section 2.2 ($C_l = 0.02$) and using double thermal losses ($C_l = 0.04$). The total energy balance for the six-year simulation is shown in Figure 5, where the time is measured in semesters. Electromagnetic waves emission is constant for six months during renewable energy storage and switched off for the next six months during the energy recovery process. The red curves show the energy recovered from the aquifer in semiannual cycles. The recovery is made during the six months in which the electromagnetic emitter is turned off, being interrupted during the electromagnetic emission period. For instance, in the first year, the total amount of energy injected into the reservoir is 287.71 GJ, while the energy recovered is 222.40 GJ. This implies that part of the energy remains in the reservoir ($C_l \geq 0$) or is lost ($C_l > 0$). The corresponding energy balance is discussed in more detail in the next section.

4.3. Energy Balance

From Figure 5, one can see that there is a difference between emitted and recovered energy. In order to evaluate this difference, Table 2 shows the relative amounts of energy recovered, stored, and lost in one-year cycles corresponding to different values of thermal losses. The data indicate that the fraction of the recovered energy increases due to the reservoir heating up. This is clearly illustrated by the ideal case (without thermal losses) where the stored energy diminishes from 18.9% to 13.2% throughout the simulations (6 years). The effect of thermal losses leads to a reduction of the recovery energy but does not affect the energy stored. For the heat losses upper bound, we consider the value $C_l = 0.04$, double the value estimated for the considered parameters. For such high thermal losses coefficient, we note that more than 69% of emitted energy can be recovered, indicating the potential efficiency of the proposed technology.

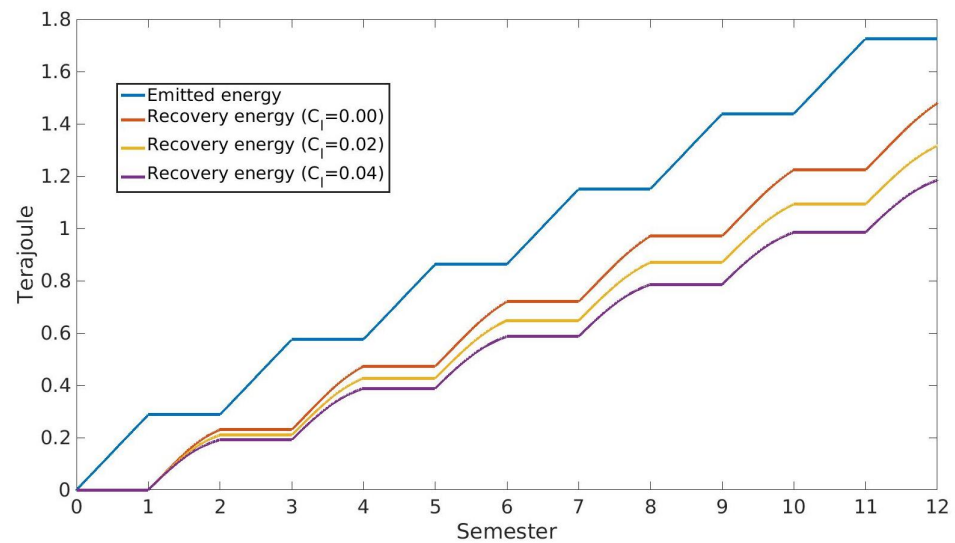


Figure 5. Comparison between the total emitted EM energy and recovered energy over time.

Table 2. Comparison of relative amounts of recovered, residual stored, and lost energy.

Yr.	$C_l = 0$			$C_l = 0.02$			$C_l = 0.04$		
	Rec.	R. St.	Lost	Rec.	R. St.	Lost	Rec.	R. St.	Lost
1	81.1%	18.9%	0%	73.8%	15.5%	10.7%	67.4%	12.7%	19.9%
2	83.2%	16.8%	0%	75.2%	12.6%	12.2%	68.3%	9.6%	22.1%
3	84.5%	15.5%	0%	76.0%	10.7%	13.3%	68.8%	7.6%	23.6%
4	85.5%	14.5%	0%	76.6%	9.2%	14.2%	69.2%	6.2%	24.6%
5	86.2%	13.8%	0%	76.9%	8.1%	15.0%	69.4%	5.2%	25.4%
6	86.8%	13.2%	0%	77.3%	7.2%	15.5%	69.5%	4.5%	26.0%

Notice that the energy required to heat the reservoir remains approximately the same, independent of the emitter power. Thus, the relative residual stored energy will be more considerable for the lower EM energy emissions, consequently diminishing the relative recovered energy.

The comparison between the proposed technique and a simple thermal energy injection rely on heat losses in the injection/production wells. In Section 4.4, we estimate the heat losses for different well sizes used in industry and different sealing materials. The estimated significant heat losses justify the EM heating technique.

4.4. Wellbore Heat Losses

Several works in the literature discuss the thermal losses in injection/production wells where water is preheated on the surface and later injected into reservoirs [39–42]. The authors concluded that thermal losses could be significant depending on the geometry and materials that make up the well and its surroundings.

The mathematical model based on Fourier’s law describes the heat flux Q_H (W) in the injection/production wellbore, which, through the tubing surface and the external composition layers (steel, cement, and rock formation), is given by

$$Q_H = 2\pi r_{to} U_{to} (\theta_h - \theta_s) \Delta H, \tag{9}$$

where r_{to} is the tubing outside radius, h is the depth, and θ_s is the formation steady temperature. The overall heat transfer U_{to} and cement/formation interface temperature θ_h are presented in [40] as

$$U_{to} = \left[\frac{r_{to} \ln(r_{to}/r_h)}{k_c} \right]^{-1} \quad \text{and} \quad \theta_h = \frac{\theta_w f(t) + \theta_s k_s / (r_{to} U_{to})}{f(t) + k_s / (r_{to} U_{to})}, \tag{10}$$

where r_h is tubing internal radius, θ_h is the cement/formation interface temperature, k_c is cement thermal conductivity, k_s is formation thermal conductivity, and $f(t) = \ln(2\sqrt{\psi t}/r_c) + 0.29$ is transient heat conduction function, where ψ is thermal diffusivity of the Earth and t is time. Following this procedure, we estimated the thermal losses for different types of wellbore (see Table 3).

Table 3. Heat losses in the wellbore during 6 months (one injection cycle).

Diameters [in]		Th. Conductivity [W/m.K]		Depth [m]	Heat Losses %
D_{tub}	D_{cas}	K_s	K_c	H	HL
5	7 3/5	1.4	0.2	1000	1.47
7 3/5	9 3/4	1.4	0.2	1000	2.18
9 3/4	20	2.8	0.4	2000	2.35
5	7 3/5	2.8	0.4	2000	5.90
9 3/4	12	1.4	0.2	1000	8.85
9 3/4	12	2.8	0.4	2000	10.6

The estimation results suggest that thermal losses in the well can be significant when the tubing diameter increases and the thickness of the cement used to fix and insulate the wellbore is thinner. In addition, the thermal conductivity of the cement and the rock formation around the well contribute to the loss of energy storage efficiency. The estimated thermal losses could exceed 10% of the energy. The electromagnetic heating method is an alternative to avoid the thermal losses during the injection process; it allows thermal energy to be stored more effectively.

5. Conclusions

We investigated heat storage into deep high-temperature aquifers by numerical simulations validated by controlled laboratory experiments. The processes are reminiscent of high-temperature energy storage (HT-ATES). The following main conclusions can be drawn from this study:

- The proposed EM heating technique could be used to produce a stable thermal front, spreading the energy through the aquifer with temperatures below the boiling point.
- Our simulation results show that even considering excessive thermal losses, the EM-heating-assisted water flooding can recover up to 70% of the stored energy. In terms of efficiency, this value is also comparable with the low-temperature ATES as reported in the literature.
- The energy balance estimate in the wellbore shows that down-hole EM heating can reduce energy losses for the deep aquifers (>1000 m), which can be notable if the water is heated at the surface.

In summary, the results discussed in this work present the use of EM-heating-assisted water flooding as a promising alternative for the storage of renewable energies in deep aquifers with high temperatures (HT-ATES).

Author Contributions: Conceptualization, G.C. and P.L.J.Z.; methodology, G.C. and S.O.d.A.; software, S.O.d.A.; validation, S.O.d.A., G.C. and P.L.J.Z.; formal analysis, S.O.d.A. and G.C.; investigation, S.O.d.A.; writing—original draft preparation, S.O.d.A., G.C. and P.L.J.Z.; writing—review and editing, S.O.d.A., G.C. and P.L.J.Z.; supervision, G.C. and P.L.J.Z. All authors have read and agreed to the published version of the manuscript.

Funding: G.C. was supported in part by CNPq grants 303245/2019-0, 405366/2021-3 and FAPEMIG grant APQ-00405-21.

Institutional Review Board Statement: Not applicable.

Informed Consent Statement: Not applicable.

Data Availability Statement: Not applicable.

Acknowledgments: The authors thank Thiago Quinelato for the assistance with the numerical algorithms.

Conflicts of Interest: The authors declare no conflict of interest. The funders had no role in the design of the study.

Appendix A. Model Validation

This validation procedure can be found in [28] (we present it here for the sake of completeness), where analytical solutions were presented and compared with laboratory experiments and numerical simulations. Analytical solutions for a similar system of equations describing the thermal–hydro coupling effect during energy extraction in geothermal reservoirs can be found in the literature (see [43,44]).

In order to validate the model presented in this paper, we retrace the laboratory-scale experiments of water injection in a porous medium under high-frequency EM heating [20]. The experiments were conducted in the presence of oil, but oil plays a passive role in comparing the model and experiments. A conventional EM microwave emitter, a conical EM wave guide, and the core-holder were placed inline in the Faraday cage to contain the radiation. The wave guide’s conical shape was specially designed to direct the emitted microwaves towards the inlet section of the core. The core structure was formed by a cylindrical case around the porous medium composed of Bentheimer Sandstone. A high-precision pump was used to inject water into the core. Fiber-optic temperature sensors were placed at a distance of 2, 5, 9, and 14 cm from the injection point.

From the set of experiments carried out, two were selected for the validation of our model. Table A1 summarizes all parameters of these experiments, which were also used in simulations. The only parameter that was not provided is the electromagnetic attenuation constant. Thus, using the data obtained by the temperature sensors and the relative data process, we can estimate its value as $\alpha = 2.8 \text{ 1/m}$.

Table A1. Physical parameters used in modeling validation.

Symbol	Physical Quantity	Exp A	Exp B	Unit (SI)
L	Reservoir length	0.17	0.17	[m]
A	Cross-section area	1.13×10^{-3}	1.13×10^{-3}	[m ²]
θ_0	Initial temperature	308.15	308.15	[K]
α	EM energy absorption	4.8	2.8	[1/m]
P	EM emitters power	45	40	[W]
D	Darcy velocity	0	2.8×10^{-4}	[m/s]
C_t	System specific heat	2.253	5.058	[MJ/m ³ ·K]
C_w	Total fluid specific heat	3.52	0.924	[MJ/m ³ ·K]
K_t	Total system thermal conduc.	1.824	1.9216	[W/m·K]
C_l	Thermal losses coefficient	0.0	7.0	[KW/m ³ ·K]

Experiment A:

In this experiment, the porous medium is completely saturated with water at room temperature. After stopping the water injection, the electromagnetic wave emitter is turned on, and the optical sensors measure the temperature over time without water flooding. For numerical simulations, we disregard the convective term of Equation (1). The boundary conditions consider the Neumann condition null on both borders. For the initial condition, we consider water’s ambient temperature. The specific parameters used in numerical simulations are given in Table A1, and the results are shown in Figure A1.

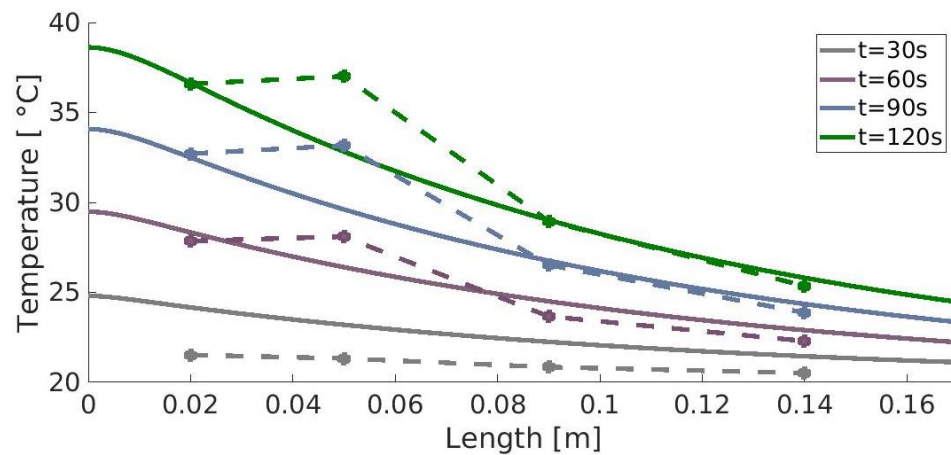


Figure A1. Temperature profiles for Experiment A (EM heating with no water flooding). The continuous lines represent the model’s solution, and the dots represent data obtained by optical thermometers [20].

Experiment B:

In this experiment, the porous medium is saturated with water and oil. Then, water is injected at a constant flow simultaneously with electromagnetic heating. For the numerical simulation, we considered the ambient water temperature as the initial condition. The boundary conditions were defined considering the Neumann condition null at the outlet and Dirichlet with a linear increase at the inlet. The specific parameters used in numerical simulations are given in Table A1, and the results are shown in Figure A2.

Notice that in Figure A1 there are differences between the experiment data and numerical simulations. The explanation, according to authors [20], is that the air inside the Faraday cage around the core begins to heat up quickly, according to Fourier’s law. They believe that this difference decreases according to the stabilization of the air temperature inside the Faraday cage with time. We believe that on the reservoir scale, especially for deep aquifers, this temperature variation is less significant.

Taking into account the experimental errors, one can observe that the proposed model captures the correct qualitative behavior observed in the experiments. This supports the overall approach adopted in our paper.

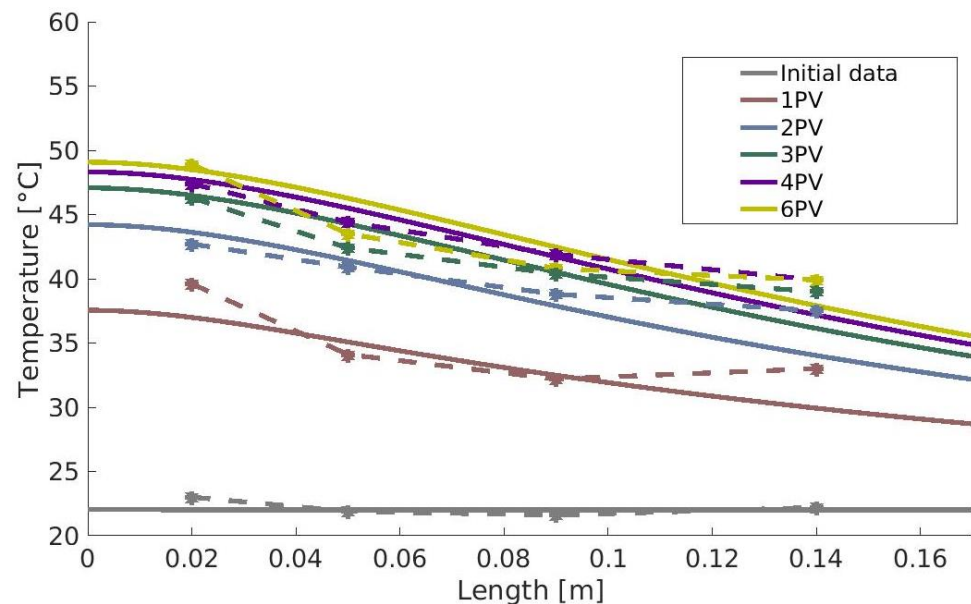


Figure A2. Temperature profiles for Experiment B (EM heating and flooding). The continuous lines represent the model’s solution, and the dots represent data obtained by optical thermometers [20].

References

1. Dorsey-Palmateer, R. Effects of wind power intermittency on generation and emissions. *Electr. J.* **2019**, *32*, 25–30. [[CrossRef](#)]
2. Dickinson, J.S.; Buik, N.; Matthews, M.C.; Sniijders, A. Aquifer thermal energy storage: Theoretical and operational analysis. *Géotechnique* **2009**, *59*, 249–260. [[CrossRef](#)]
3. Sommer, W. Modelling and Monitoring of Aquifer Thermal Energy Storage: Impacts of Soil Heterogeneity, Thermal Interference and Bioremediation. Ph.D. Thesis, Wageningen University, Wageningen, The Netherlands, 2015.
4. Kallesøe, A.; Vangkilde-Pedersen, T. HEATSTORE—Underground Thermal Energy Storage (UTES)—State of the Art, Example Cases and Lessons Learned. In Proceedings of the World Geothermal Congress, Reykjavik, Iceland, 24–27 October 2020.
5. Fleuchaus, P.; Schüppler, S.; Bloemendal, M.; Guglielmetti, L.; Opel, O.; Blum, P. Risk analysis of High-Temperature Aquifer Thermal Energy Storage (HT-ATES). *Renew. Sustain. Energy Rev.* **2020**, *133*, 110153. [[CrossRef](#)]
6. Kastner, O.; Norden, B.; Klapperer, S.; Park, S.; Urpi, L.; Cacace, M.; Blöcher, G. Thermal solar energy storage in Jurassic aquifers in Northeastern Germany: A simulation study. *Renew. Energy* **2017**, *104*, 290–306. [[CrossRef](#)]
7. Schmidt, T.; Müller-Steinhagen, H. Die solar unterstützte Nahwärmeversorgung mit saisonalem Aquifer-Wärmespeicher in Rostock—Ergebnisse nach vier Betriebsjahren. In *Symposium Erdgekoppelte Wärmepumpen; Geothermische Fachtagung*; Landau, Germany, 2004.
8. Kangas, M.; Lund, P. Modeling and simulation of aquifer storage energy systems. *Sol. Energy* **1994**, *53*, 237–247. [[CrossRef](#)]
9. Ghaebi, H.; Bahadori, M.; Saidi, M. Performance analysis and parametric study of thermal energy storage in an aquifer coupled with a heat pump and solar collectors, for a residential complex in Tehran, Iran. *Appl. Therm. Eng.* **2014**, *62*, 156–170. [[CrossRef](#)]
10. Badakhshan, S.; Hajibandeh, N.; Shafie-khah, M.; Catalão, J. Impact of solar energy on the integrated operation of electricity-gas grids. *Energy* **2019**, *183*, 844–853. [[CrossRef](#)]
11. Lau, D.; Song, N.; Hall, C.; Jiang, Y.; Lim, S.; Perez-Wurfl, I.; Ouyang, Z.; Lennon, A. Hybrid solar energy harvesting and storage devices: The promises and challenges. *Mater. Today Energy* **2019**, *13*, 22–44. [[CrossRef](#)]
12. Wilberforce, T.; Baroutaji, A.; El Hassan, Z.; Thompson, J.; Soudan, B.; Olabi, A.G. Prospects and challenges of concentrated solar photovoltaics and enhanced geothermal energy technologies. *Sci. Total Environ.* **2019**, *659*, 851–861. [[CrossRef](#)]
13. Bera, A.; Babadagli, T. Status of electromagnetic heating for enhanced heavy oil/bitumen recovery and future prospects: A review. *Appl. Energy* **2015**, *151*, 206–226. [[CrossRef](#)]
14. Shafiai, S.; Gohari, A. Conventional and electrical EOR review: The development trend of ultrasonic application in EOR. *J. Pet. Explor. Prod. Technol.* **2020**, *10*, 2923–2945. [[CrossRef](#)]
15. Sivakumar, P.; Krishna, S.; Hari, S.; Vij, R. Electromagnetic heating, an eco-friendly method to enhance heavy oil production: A review of recent advancements. *Environ. Technol. Innov.* **2020**, *20*, 101100. [[CrossRef](#)]
16. Hasanvand, M.Z.; Golparvar, A. A Critical Review of Improved Oil Recovery by Electromagnetic Heating. *Pet. Sci. Technol.* **2014**, *32*, 631–637. [[CrossRef](#)]
17. Pizarro, J.; Trevisan, O. Electrical heating of oil reservoirs: Numerical simulation and field test results. *J. Pet. Technol.* **1990**, *42*, 1–320. [[CrossRef](#)]
18. Sahni, A.; Kumar, M.; Knapp, R.B. Electromagnetic heating methods for heavy oil reservoirs. In Proceedings of the Western Regional Meeting, SPE/AAPG, Long Beach, CA, USA, 19–23 June 2000; pp. 19–23.
19. Chhetri, A.; Islam, M. A critical review of electromagnetic heating for enhanced oil recovery. *Pet. Sci. Technol.* **2008**, *26*, 1619–1631. [[CrossRef](#)]
20. Paz, P.; Hollmann, T.; Kermen, E.; Chapiro, G.; Slob, E.; Zitha, P. EM Heating-Stimulated Water Flooding for Medium–Heavy Oil Recovery. *Transp. Porous Media* **2017**, *119*, 57–75. [[CrossRef](#)]
21. Cerutti, A.; Bandinelli, M.; Bientinesi, M.; Petarca, L.; De Simoni, M.; Manotti, M.; Maddinelli, G. A New Technique for Heavy Oil Recovery Based on Electromagnetic Heating: System Design and Numerical Modelling. *Chem. Eng. Trans.* **2013**, *32*, 1255–1260.
22. Jha, A.K.; Joshi, N.; Singh, A. Applicability and Assessment of Micro-Wave Assisted Gravity Drainage (MWAGD) Applications in Mehsana Heavy Oil Field. In Proceedings of the SPE Heavy Oil Conference and Exhibition, Kuwait City, Kuwait, 12–14 December 2011; pp. 11–14.
23. Mukhametshina, A.; Martynov, E. Electromagnetic Heating of Heavy Oil and Bitumen: A Review of Experimental Studies and Field Applications. *J. Pet. Eng.* **2013**, *2013*, 476519. [[CrossRef](#)]
24. Eskandari, S.; Jalalhosseini, S.M.; Mortezaazadeh, E. Microwave Heating as an Enhanced Oil Recovery Method—Potentials and Effective Parameters. *Energy Sources Part A Recovery Util. Environ. Eff.* **2015**, *37*, 742–749. [[CrossRef](#)]
25. Soliman, M. Approximate solutions for flow of oil heated using microwaves. *J. Pet. Sci. Eng.* **1997**, *18*, 93–100. [[CrossRef](#)]
26. Rubinstein, L. The total heat losses in injection of hot liquid into a stratum. *Neft. Gaz* **1959**, *9*, 41.
27. Carrizales, M.A.; Lake, L.W.; Johns, R.T. Multiphase fluid flow simulation of heavy oil recovery by electromagnetic heating. In *SPE IOR Symposium*; OnePetro: Richardson, TX, USA, 2010.
28. Almeida, S.O.; Zitha, P.L.J.; Chapiro, G. A method for analyzing electromagnetic heating assisted water flooding process for heavy oil recovery. *Transp. Porous Media* **2021**. [[CrossRef](#)]
29. Fanchi, J.R. Feasibility of reservoir heating by electromagnetic irradiation. In Proceedings of the SPE Annual Technical Conference and Exhibition, New Orleans, LA, USA, 23–26 September 1990.
30. Darcy, H. *Les Fontaines Publiques de la Ville de Dijon*; Victor Dalmond: Paris, France, 1856.
31. Whitaker, S. The equations of motion in porous media. *Chem. Eng. Sci.* **1966**, *21*, 291–300. [[CrossRef](#)]

32. Viswanath, D.; Ghosh, T.; Prasad, D.; Dutt, N.; Rani, K. *Viscosity of Liquids: Theory, Estimation, Experiment, and Data*; Springer: Dordrecht, The Netherlands, 2007.
33. Chen, Z.; Huan, G.; Ma, Y. *Computational Methods for Multiphase Flows in Porous Media (Computational Science and Engineering 2)*; SIAM: Philadelphia, PA, USA, 2006.
34. Kaviany, M. *Principles of Heat Transfer in Porous Media*; Springer: Berlin/Heidelberg, Germany, 1991.
35. Sudiko, M. *Elementes of Electromagnetics*; Oxford University Press: New York, NY, USA, 2014.
36. Stratton, J.A. *Electromagnetic Theory*; McGraw-Hill: New York, NY, USA, 1941.
37. Hughes, T.; Franca, P.; Hulbert, G. A new finite element formulation for computational fluid dynamics: VIII. The galerkin/least-squares method for advective-diffusive equations. *Comput. Methods Appl. Mech. Eng.* **1989**, *73*, 173–189. [[CrossRef](#)]
38. Settari, A.; Walters, D. Advances in Coupled Geomechanical and Reservoir Modeling With Applications to Reservoir Compaction. *SPE J.* **2001**, *6*, 334–342. [[CrossRef](#)]
39. Ramey, H.J., Jr. Wellbore Heat Transmission. *J. Pet. Technol.* **1962**, *14*, 427–435. [[CrossRef](#)]
40. Willhite, G. Over-all Heat Transfer Coefficients in Steam And Hot Water Injection Wells. *J. Pet. Technol.* **1967**, *19*, 607–615. [[CrossRef](#)]
41. Cheng, W.L.; Han, B.B.; Nian, Y.L.; Wang, C.L. Study on wellbore heat loss during hot water with multiple fluids injection in offshore well. *Appl. Therm. Eng.* **2016**, *95*, 247–263. [[CrossRef](#)]
42. Ameli, F.; Alashkar, A.; Hemmati-Sarapardeh, A. *Thermal Recovery Processes*; Elsevier: Amsterdam, The Netherlands, 2018; pp. 139–186.
43. Fan, Z.; Parashar, R. Analytical Solutions for a Wellbore Subjected to a Non-isothermal Fluid Flux: Implications for Optimizing Injection Rates, Fracture Reactivation, and EGS Hydraulic Stimulation. *Rock Mech. Rock Eng.* **2019**, *52*, 4715–4729. [[CrossRef](#)]
44. Fan, Z.; Parashar, R.; Jin, Z.H. Impact of convective cooling on pore pressure and stresses around a borehole subjected to a constant flux: Implications for hydraulic tests in an enhanced geothermal system reservoir. *Interpretation* **2020**, *8*, SG13–SG20. [[CrossRef](#)]